Localization and scaling properties of magnetostatic modes in quasiperiodic magnetic superlattices



2000 J. Phys.: Condens. Matter 12 1041

(http://iopscience.iop.org/0953-8984/12/6/322)

J. Phys.: Condens. Matter **12** (2000) 1041–1052. Printed in the UK PII: S0953-8984(00)05105-5

# Localization and scaling properties of magnetostatic modes in quasiperiodic magnetic superlattices

Dory H A L Anselmo†‡, M G Cottam† and E L Albuquerque‡

† Department of Physics and Astronomy, University of Western Ontario, London, Ontario, Canada N6A 3K7

‡ Departamento de Física, Universidade Federal do Rio Grande do Norte, Natal-RN, 59072-970 Brazil

Received 10 June 1999, in final form 26 October 1999

**Abstract.** The localization and scaling behaviour of quasiperiodic structures are studied for a geometry where the magnetization is perpendicular to the interfaces of the superlattices. Numerical results for the bulk and surface spin waves in the magnetostatic regime are presented for the Fibonacci, Thue–Morse and period-doubling sequences. The results are obtained for both ferromagnetic and antiferromagnetic ordering by using the transfer-matrix method. Interesting features of the localized modes are shown for Fe, EuS and $MnF_2$.

## 1. Introduction

Since the discovery of the icosahedral phase in Al–Mn alloys by Shechtman *et al* [1], the field of quasiperiodic structures (or quasicrystals) has caught a lot of attention. Several studies have been made on these structures, for the electronic [2–7] and phonon [2,8] modes. Experimental and theoretical results have been reported for different kinds of quasiperiodic structure, such as Fibonacci [9, 10], Thue–Morse [11–13] and period doubling [14]. However, while these results were related mainly to electronic and structure properties, little progress has been made in experimental studies of non-periodic structures in the regime of magnetostatic modes.

The term *quasicrystal* is more appropriate for natural compounds or artificial alloys, although in one dimension there is no difference between this and the quasiperiodic structure formed by the incommensurate arrangement of periodic unit cells [9]. An appealing motivation for studying these structures is that they exhibit a highly fragmented energy spectrum displaying a self-similar pattern. Indeed, from a strictly mathematical perspective, it has been proven that their spectra are Cantor sets in the thermodynamic limit [15, 16].

With advances in multilayer fabrication (including epitaxial deposition [9], among other methods) and in characterization techniques, such as x-ray scattering or neutron diffraction, it is possible to reveal novel features of such structures. Also, several different mathematical techniques including renormalization group [17, 18] and transfer-matrix [19, 20] methods have been successfully applied, leading to remarkable results. For example, for the Thue–Morse spectrum, it is known that the structure factor is composed of a sequence of $\delta$-peaks [21], although they do not scale like $L^2$, $L$ being the typical length of the system. In this case, there are some conflicting results. Some authors [20] argue that the results in the case of the electronic properties of the Thue–Morse sequence should depend on the nature of the model.

0953-8984/00/061041+12$30.00  

However, this is not conclusively established and it may not apply in the case of magnetic properties.

Spin-wave spectra in quasiperiodic magnetic structures have been recently investigated, by considering the nature of the solutions for the appropriate wave field in each film. The modes in these structures are coupled across the interfaces (through boundary conditions), and are calculated with the assistance of Bloch's theorem, where appropriate. The surfaces and interfaces in these layered structures play an important role in the properties of the entire system and for the excitations in particular. Many of the previous works have been concerned with the spin-wave excitations in the low-temperature regime, where at least one of the components is a ferromagnetic or an antiferromagnetic material. Furthermore, depending on the relative importance of the magnetic dipole–dipole and exchange interactions, different models for the magnetic behaviour can be employed. For instance, for sufficiently small values of the excitation wavevector ($k \lesssim 10^7$ m$^{-1}$), dipolar effects are dominant and magnetostatic modes should propagate in such superlattices [22–24]. On the other hand, at larger excitation wavevectors, typically $k \gtrsim 10^8$ m$^{-1}$ in a ferromagnet, the exchange interaction, which is the restoring force for spin waves, will be dominant [24, 25].

It is our aim in this work to investigate the magnetostatic modes in quasiperiodic structures made up of magnetic and non-magnetic materials. By contrast to the case considered in references [19] and [21], in which the authors consider the geometry where the wavevector and the applied field are in the same plane (Voigt geometry), we consider here an in-plane wavevector and an applied field $H_0$ and magnetization (or sublattice magnetization for an antiferromagnet) in the direction perpendicular to the interfaces. Our model is based on a transfer-matrix formalism, to simplify the algebra, which is otherwise quite involved. The localization and scaling properties of the spectra are also presented and discussed.

The remainder of this paper is organized as follows. The basic definitions of our structures and the mathematical outline are given in section 2. In section 3 we present some results regarding the spin-wave excitations in different sequences, as well as different magnetic materials. Finally, in section 4 we conclude and suggest some possible extensions of our results.

## 2. Theoretical model

In the magnetostatic regime Maxwell's equations give

$$\nabla \cdot \boldsymbol{B} = 0 \tag{1}$$

$$\nabla \times \boldsymbol{h} = 0 \tag{2}$$

where $\boldsymbol{B}$ and $\boldsymbol{h}$ are related by the constitutive tensorial equation $\boldsymbol{B} = \overleftrightarrow{\mu}\boldsymbol{h}$, and $\overleftrightarrow{\mu}$ is the permeability tensor. Here, we assume a temporal dependence $\exp(-\mathrm{i}\omega t)$ for the fluctuating fields, and the form of the matrix $\overleftrightarrow{\mu}$ for a uniaxial material is

$$\overleftrightarrow{\mu} = \begin{bmatrix} \mu_1 & \mathrm{i}\mu_2 & 0 \\ -\mathrm{i}\mu_2 & \mu_1 & 0 \\ 0 & 0 & 1 \end{bmatrix}. \tag{3}$$

One can show [27] that for a ferromagnetic material

$$\mu_1 = 1 + \frac{4\pi\gamma^2 H_i M}{\gamma^2 H_i^2 - \omega^2} \tag{4}$$

$$\mu_2 = \frac{4\pi\gamma\omega M}{\gamma^2 H_i^2 - \omega^2} \tag{5}$$

where $H_i$ is the internal magnetic field in the $z$-direction, given by $H_i = H_0 - 4\pi M$. Also, $H_0$ is the external applied field, $M$ is the saturation magnetization and $\gamma$ is the gyromagnetic ratio. When $M$ is perpendicular to the surface, as in our case here, it gives rise to depolarizing fields, and this is the reason for a decrease in the net magnetic field inside the material. For an antiferromagnet we have

$$\mu_1 = 1 + \frac{4\pi\gamma^2 H_A M}{\omega_0^2 - (\omega + \gamma H_0)^2} + \frac{4\pi\gamma^2 H_A M}{\omega_0^2 - (\omega - \gamma H_0)^2} \tag{6}$$

$$\mu_2 = \frac{4\pi\gamma^2 H_A M}{\omega_0^2 - (\omega + \gamma H_0)^2} - \frac{4\pi\gamma^2 H_A M}{\omega_0^2 - (\omega - \gamma H_0)^2} \tag{7}$$

where

$$\omega_0 = |\gamma|[H_A(2H_E + H_A)]^{1/2}. \tag{8}$$

Here $H_E$ is the effective exchange field and $H_A$ is the anisotropy field. For this case, $M$ is the saturation magnetization of one of the sublattices, and the physical parameter $\omega_0$ is the so-called antiferromagnetic resonance frequency in zero applied field. The equations of motion are derived as follows. From (1) and (2), we can define a magnetic scalar potential $\phi$, by $\boldsymbol{h} = -\boldsymbol{\nabla}\phi$. Using this together with (3), we obtain the expression

$$\left[\mu_1\left(\frac{\partial^2}{\partial x^2} + \frac{\partial^2}{\partial y^2}\right) + \frac{\partial^2}{\partial z^2}\right]\phi = 0. \tag{9}$$

This equation is valid for both the magnetic and non-magnetic layers of a superlattice (but in the latter case, $\overleftrightarrow{\mu} = \mathbf{I}$, the identity matrix). By considering solutions of the form

$$\phi = \phi(z)\mathrm{e}^{\mathrm{i}(kx - wt)} \tag{10}$$

where $k$ is a wavevector (taken in the $x$-direction) parallel to the surface, and substituting into (9), one gets

$$\left(-\mu_1 k^2 + \frac{\mathrm{d}^2}{\mathrm{d}z^2}\right)\phi(z) = 0. \tag{11}$$

The above equation has solutions of the form $\phi(z) = A\mathrm{e}^{\alpha z} + B\mathrm{e}^{-\alpha z}$, where $\alpha$ may be complex and is directly related to $k$ by $\alpha = (\mu_1)^{1/2}k$. We need to impose some boundary conditions at interfaces in the layered structure, and this leads us to the requirement that both $\phi$ and $\partial\phi/\partial z$ must be continuous at any interface. By applying the boundary conditions, together with the above set of equations, we obtain implicit expressions for the dispersion relations. In previous work [28] on periodic structures it was shown that we need only consider $\mu_1 < 0$ in order to obtain the bulk and surface modes. This has the consequence that for a ferromagnet, the range of frequencies is $|\gamma|H_i < \omega < |\gamma|(H_i H_0)^{1/2}$, while for an antiferromagnet with zero applied field, the frequencies are confined to the range $\omega_0 < \omega < (\omega_0^2 + 8\pi\gamma^2 H_A M)^{1/2}$.

In order to construct the quasiperiodic superlattices, we define briefly here the rules of the unit-cell growth; the unit cell consists of a sequence of building blocks (or layers), where the arrangement of the layers follows the desired sequence. For the well-known Fibonacci (FB) sequence, the rule is $S_n = S_{n-1}S_{n-2}$, $n > 2$, where $S_1 = \mathrm{A}$, $S_2 = \mathrm{AB}$. The FB rule is invariant under the transformation $\mathrm{A} \rightarrow \mathrm{AB}$ and $\mathrm{B} \rightarrow \mathrm{A}$. For the Thue–Morse (TM) sequence, the rule of growth is defined by $S_n = S_{n-1}S_{n-1}^+$, $S_n^+ = S_{n-1}^+ S_{n-1}$, with $n \geqslant 1$ and $S_0 = \mathrm{A}$ and $S_0^+ = \mathrm{B}$. Alternatively, this sequence can be grown following the inflation rules $\mathrm{A} \rightarrow \mathrm{AB}$ and $\mathrm{B} \rightarrow \mathrm{BA}$. Finally, for the period-doubling (PD) sequence, we have $S_n = S_{n-1}S_{n-1}^+$, $S_n^+ = S_{n-1}S_{n-1}$, $n \geqslant 1$, also with $S_0 = \mathrm{A}$ and $S_0^+ = \mathrm{B}$. The inflation rules for this sequence

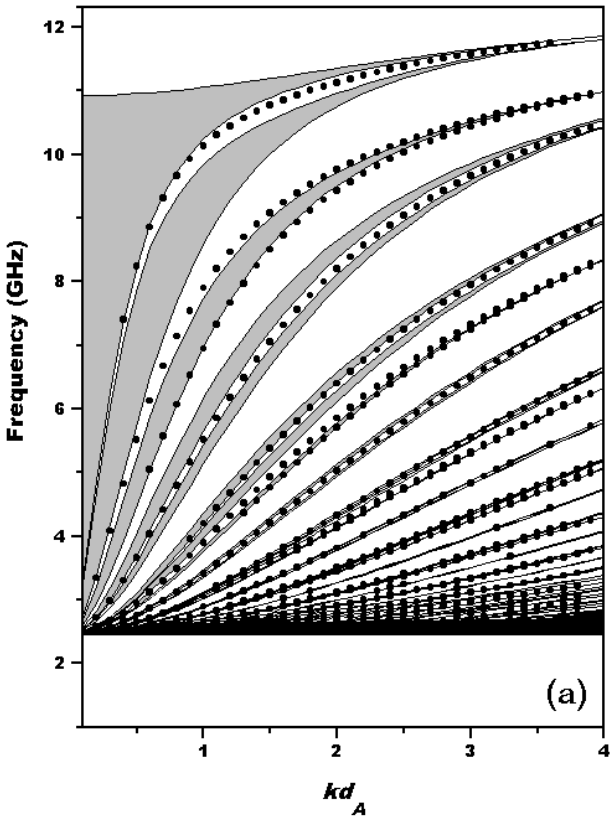


**Figure 1.** Magnetostatic bulk (shaded areas) and surface (dotted lines) modes for some quasi-periodic structures: (a) the fifth generation of the Fibonacci sequence; the magnetic material is Fe, and the physical parameters used here are $H_0 = 22$ kG, $M = 1.68$ kG and $R = 0.5$; (b) the third generation of the period-doubling sequence; here the magnetic material is the antiferromagnet $MnF_2$, with physical parameters given by $H_0 = 0.15$ kG, $M = 0.6$ kG, $H_E = 550$ kG, $H_A = 7.78$ kG and $R = 0.5$.

are A $\rightarrow$ AB and B $\rightarrow$ AA. All these inflation rules can also be understood as an invariance condition, because they leave their respective sequences invariant when applied.

The number of blocks for the FB sequence increases with the so-called Fibonacci number $F_n$, defined by $F_n = F_{n-1} + F_{n-2}$ (considering the initial conditions $F_0 = F_1 = 1$). For the TM and PD sequences the size of the unit cell increases as a function of the sequence generation, namely as $2^n$. As we shall see, this dependence has the consequence that for the TM and PD sequences, the localization of the modes is stronger for lower values of the generation number.

In the above definitions, the layers A and B consist respectively of a magnetic material having thickness $d_{\mathrm{A}}$ and a non-magnetic one having thickness $d_{\mathrm{B}}$. The physical properties of such materials are included in the definitions of $\mu_1$ and $\mu_2$. The external field $H_0$ in our calculations is applied in the $z$-direction, which is perpendicular to the interfaces. This causes the modes to behave quite differently from the case of the Voigt geometry [22,24]. In particular, the Damon–Eshbach modes do not occur in our geometry, and there are multiple branches in the spin-wave spectrum (e.g. see reference [26] for the case of periodic superlattices).

In magnetic quasiperiodic superlattices a relevant quantity is the ratio between the numbers of magnetic and non-magnetic building blocks. For the FB sequence, as the sequence number

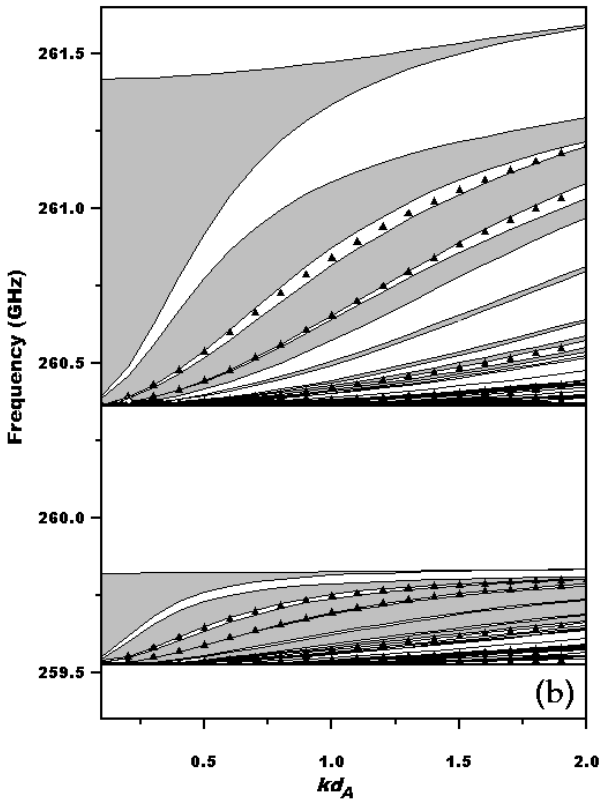


**Figure 1.** (Continued)

tends to infinity, this ratio tends to the *golden mean*, $\frac{1}{2}(1+\sqrt{5}) \simeq 1.618$. For the TM sequence, this ratio is constant and is equal to unity, but for the PD sequence this ratio is not constant, and actually tends to 2 when $n \to \infty$.

Now we apply our theory to the superlattices. Inside a layer A we consider solutions of the type

$$\phi(z) = A_+ \mathrm{e}^{\alpha z} + A_- \mathrm{e}^{-\alpha z} \tag{12}$$

and for a layer B

$$\phi(z) = B_+ \mathrm{e}^{kz} + B_- \mathrm{e}^{-kz}. \tag{13}$$

Using these solutions, and defining $L = n_\mathrm{A} d_\mathrm{A} + n_\mathrm{B} d_\mathrm{B}$ as the length of the unit cell, we apply the boundary conditions (the continuity of $\phi$ and $\partial\phi/\partial z$) at the interfaces. The resulting equations can be cast in a matrix form, involving the transfer matrix $\mathbf{T}$ of the problem, which contains information describing the structure generated for a particular sequence. It can be used to study the behaviour of the bulk and (when applied in an appropriate manner) the surface modes. After some algebra we find that

$$|\mathbf{A}^{n+1}\rangle = \mathbf{T}|\mathbf{A}^n\rangle \tag{14}$$

where $|\mathbf{A}^n\rangle$ is a column matrix of the amplitudes $A_\pm$ in the $n$th cell. The explicit form of the transfer matrix is given in appendix A. A quasiperiodic superlattice is a structure whose unit cell is formed using a non-periodic rule of growth. These unit cells are then stacked

periodically to form a superlattice. In these terms, Bloch's theorem is still applicable, giving

$$|\mathbf{A}^{n+1}\rangle = \mathrm{e}^{\mathrm{i}QL}|\mathbf{A}^{n}\rangle \tag{15}$$

where $Q$ is a real wavevector of the infinite superlattice. Using (14) and (15), the implicit dispersion relation can be expanded as

$$\cos(QL) = \frac{1}{2}\,\mathrm{Tr}(\mathbf{T}). \tag{16}$$

If we consider now a semi-infinite superlattice (constructed in the region $z \geqslant 0$), we can still use equation (16), but we must deal with, in addition to the bulk modes with $Q$ real, surface modes with $Q$ complex of the form $Q \equiv \mathrm{i}\beta$. For the surface modes, equations (14) and (15) read

$$T_{11} + \lambda^{-1}T_{12} = \mathrm{e}^{-\beta L} = T_{22} + \lambda T_{21} \tag{17}$$

where $\lambda = (\alpha + k)/(\alpha - k)$, and the constant $\beta$ must be chosen such that $\mathrm{Re}(\beta) > 0$. If we define the quantity $x_j \equiv \frac{1}{2}\,\mathrm{Tr}(\mathbf{T}_j)$, where $\mathbf{T}_j$ stands for the transfer matrix describing the $j$th-generation superlattice, one can show [3] that for the FB sequence $x_j$ obeys the recursion relation

$$x_{j+1} = 2x_j x_{j-1} - x_{j-2}. \tag{18}$$

The expression above can be understood as a 3D tracing map, as can be seen from the transformation

$$\boldsymbol{r}_{j+1} = \mathbf{T}\boldsymbol{r}_j = (2x_j y_j - z_j, x_j, y_j) \tag{19}$$

where $\boldsymbol{r}_j$ is a vector defined by $\boldsymbol{r}_j = (x_j, x_{j-1}, x_{j-2}) = (x_j, y_j, z_j)$. The quantity

$$I = x_{j+1}^2 + x_j^2 + x_{j-1}^2 - 2x_{j+1}x_j x_{j-1} - 1 \tag{20}$$

can be shown to be independent of the mapping (19) (i.e. independent of $j$), by using equation (18).

## 3. Numerical results

We now apply our calculations to some specific magnetic materials. We define $R = d_{\mathrm{B}}/d_{\mathrm{A}}$ as the ratio between the thicknesses of the non-magnetic and the magnetic layers, respectively. The spectra $\omega$ versus $kd_{\mathrm{A}}$ of the spin waves in the magnetostatic regime are shown in figure 1. Starting with the ferromagnetic case in figure 1(a), we consider the magnetic material A as Fe, for the fifth generation of the FB sequence. The physical parameters used here are: for Fe [28] $H_0 = 22$ kG, $M = 1.68$ kG and $R = 0.5$; and for EuS $H_0 = 13.5$ kG and $M = 1.0$ kG. On the other hand, we consider $MnF_2$ as the antiferromagnetic material, whose physical parameters are [28]: $H_0 = 0.15$ kG, $M = 0.6$ kG, $H_E = 550$ kG and $H_A = 7.78$ kG. As one can see clearly in this and in the subsequent figures, we have a well-defined lower limit for the spectra, for all values of the generation number and for all the different sequences. This happens when we approach the frequency value ($\omega \simeq 2.48$ GHz for the FB sequence, with the parameters specified here for Fe) for which we have the limit $\mu_1 \to -\infty$. Also, there is an alternation of the sequence of the roots for the boundaries of the bulk bands, as in reference [29]. For the surface modes, which exist in the forbidden region of the spectra, corresponding to the imaginary value of the Bloch wavevector, whenever one considers the sequence generation number $n > 2$, we have a natural broken symmetry for the structure. This fact implies that we do not need to vary the thickness of the magnetic (or non-magnetic) materials in order to obtain these modes [29], and this was also obeyed by all the sequences. However, we must

be careful to impose the condition $\mathrm{Re}(\beta) > 0$ in equation (17), because otherwise we can obtain non-physical surface modes. Such modes are characterized by having an amplitude with exponential *increasing*, and must therefore be excluded. In figure 1(b) we show the spectra for the antiferromagnet $MnF_2$, for the third generation of the PD sequence. In this case the existence of an applied field gives rise to a gap between two regions of real solutions for the bulk and surface modes (or with $\mu_1 < 0$). If we set the external field equal to zero, the two regions collapse into one, still showing the same self-similar behaviour as in the previous case. Also, the modes are sensitive to the value of the anisotropy field, having their relative position governed by the magnitude of $H_A$. In both figures cited above, the limits of the bands are given by $QL = 0$ and $QL = \pi$, such that we have an alternation from one band to another, following the sequence $0, \pi, \pi, 0, 0, \pi, \pi, 0, \ldots$, starting from the upper band. Also, we do not need to explicitly calculate the value of $\beta$ for the surface modes, since we just need the condition $\mathrm{Re}(\beta) > 0$ to ensure physical solutions.

Figure 2(a) and figure 2(b) show the distribution of the magnetostatic bandwidths for high generation numbers, which gives a good insight into their localization. From there we can infer the forbidden and allowed modes as a function of the generation number $N$. For large $N$ the allowed band regions get narrow and narrower, as an indication of more localized modes. One can see clearly that this has a Cantor-like behaviour, and we observed the same structure for the other sequences. For example, in figure 2(b) we show a similar spectrum, but now for the TM sequence, considering the antiferromagnet $MnF_2$. As we have observed in other sequences, there is a splitting of the spectra into two regions, governed by the magnitude of the applied magnetic field $H_0$. It can also be noticed that there exists a self-similarity between the two regions for real solutions, and for both figures there exists a strong localization when one goes

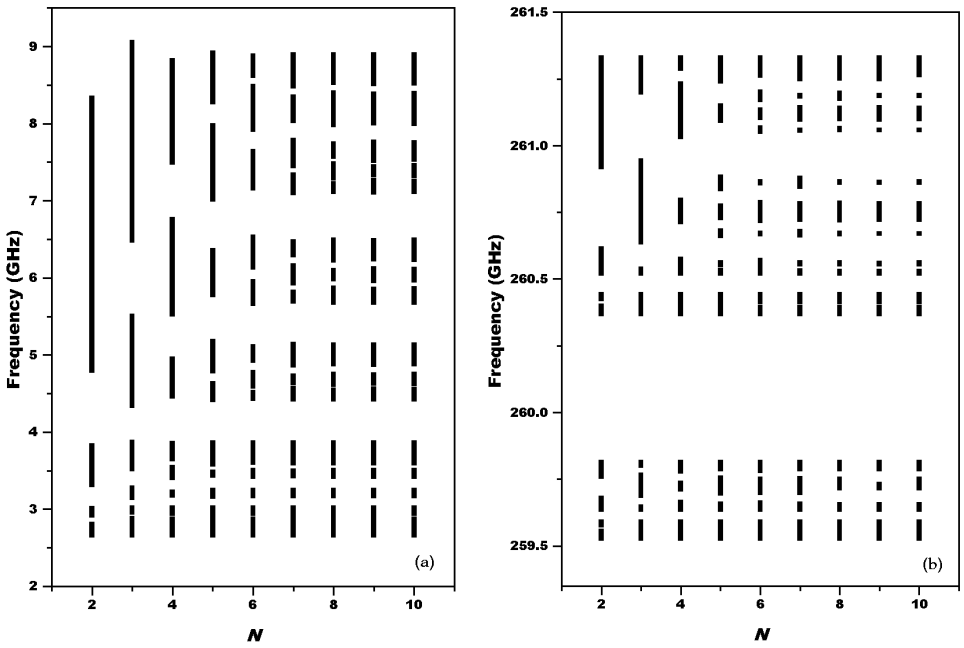


**Figure 2.** The distribution of the bandwidths as a function of the quasiperiodic generation numbers: (a) the Fibonacci sequence; the magnetic material used here is the ferromagnet EuS, with $H_0 = 13.5$ kG, $M = 1.0$ kG, $kd_\mathrm{A} = 1.0$ and $R = 0.5$; (b) the Thue–Morse sequence; the magnetic material is the antiferromagnet $MnF_2$, with the physical parameters as for figure 1(b).

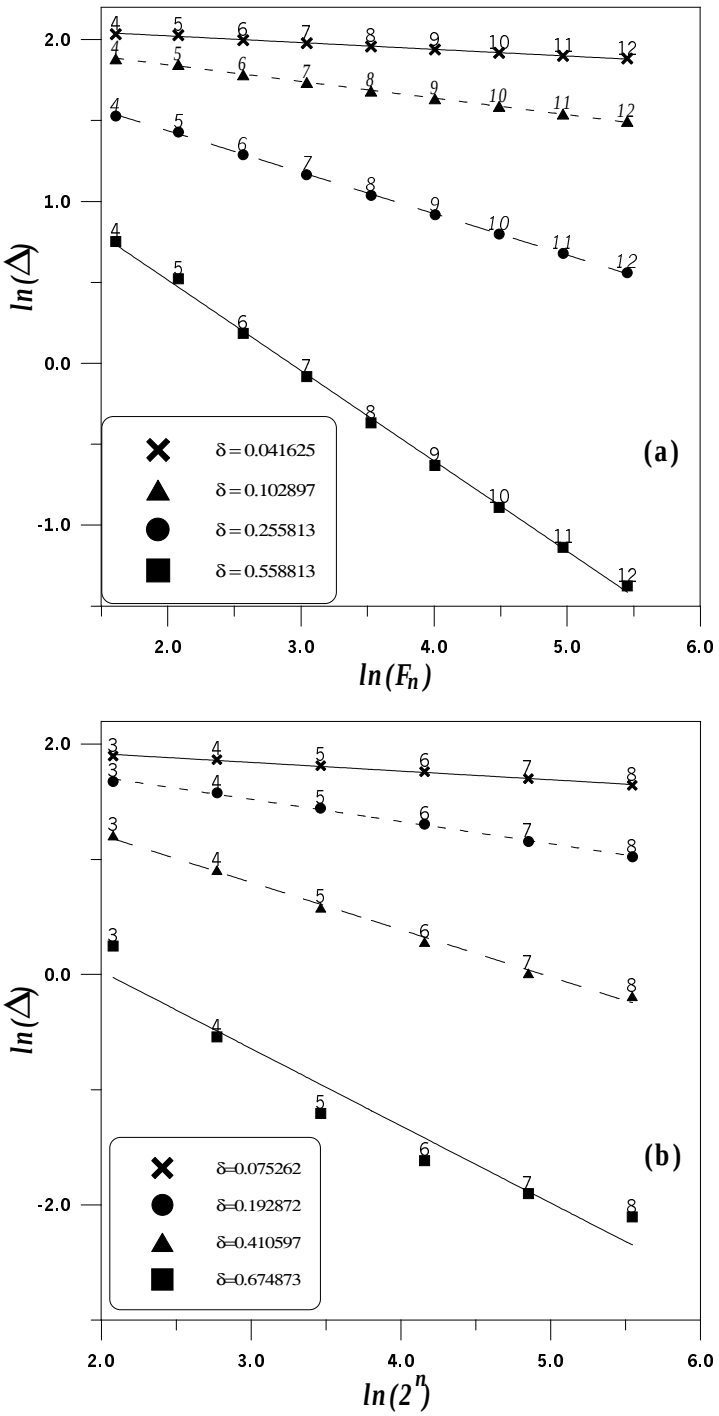


**Figure 3.** Scaling behaviour for the magnetostatic bulk modes: (a) the Fibonacci sequence; (b) the Thue–Morse sequence; (c) the period-doubling sequence. The magnetic material for all quasiperiodic systems here is considered to be Fe, and the physical parameters are the same as in previous figures. The values of $\delta$ for each of the wavenumbers are given in the insets.

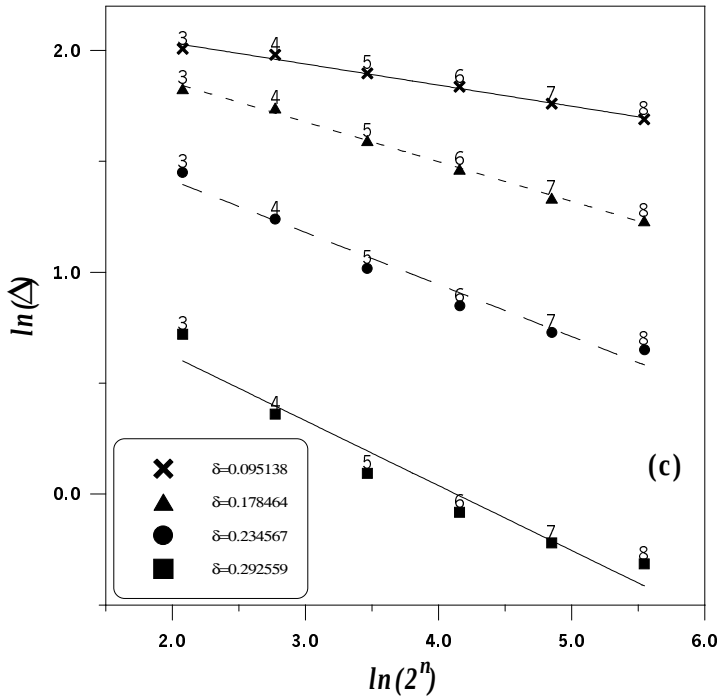


**Figure 3.** (Continued)

to higher values of the generation number (because of the limitation on what can be printed, the regions get so narrow and close together that is difficult to see this feature). It has been reported [30] that there exists a class of quasiperiodic potentials that do not exhibit localized states (i.e. they can only have continuous spectra), but in that case the authors excluded the golden mean, while in our case it appears naturally for the FB sequence.

The log–log plot of the bandwidths $\Delta$ against the generation number for the FB sequence is shown in figure 3(a). The labels at each of the points refer to the index $n$ of the generation. In each figure, the magnitudes of the in-plane wavevector are represented by different symbols. The crosses refer to $kd_{\mathrm{A}} = 0.25$, the triangles to $kd_{\mathrm{A}} = 0.5$, the circles to $kd_{\mathrm{A}} = 1.0$ and the squares to $k = 2.0$. In figure 3(b) the same log–log graph is shown, but now for the TM chain, and the scale behaviour for the PD sequence is depicted in figure 3(c). For the FB sequence, the scaling law is $\Delta \sim (F_n)^{-\delta}$, while for the TM and PD sequences, the bandwidths scale as $(2^n)^{-\delta}$. For the TM sequence, we see a stronger dependence of $\delta$ on the in-plane wavevector, compared to the case for the FB sequence, in the sense that the values of $\delta$ are higher for the same value of $k$. Observe that the linear behaviour for all sequences is not well fitted for lower values of the generation numbers of the quasiperiodic structures (2 and 3 for FB, 1 and 2 for TM and PD). The reason for this is that this linear scaling is a typical property of a fractal system, and low values of the generation number $n$ do not yet have a mark of quasiperiodicity. For example, the FB unit cell for $n = 2$ is AB (the pure periodic superlattice unit cell), and for $n = 3$ it is ABA, which gives a behaviour for the bulk modes quite similar to that of the second generation, replacing A $\rightarrow$ 2A. On the other hand, when one increases the value of $n$, one gets a fast increase of the number of the branches in all sequences and, therefore, it causes a loss of precision for the lower region of the spectra, due to the limiting behaviour of $\mu_1$.

## 4. Conclusions

In summary, we have obtained the bulk and surface solutions for the magnetostatic modes in quasiperiodic structures, where the magnetization is perpendicular to the interfaces. Different kinds of quasiperiodic system were considered. For the dispersion curves of the PD (figure 1(b)) and TM (figure 2(b)) sequences, the strong fragmentation of the bulk bands for higher values of the generation number caused a loss of precision for $k > 2.0$ (mainly for the PD sequence), so we considered this value as a good upper limit for the in-plane wavevector. For the antiferromagnetic modes with non-zero applied field the two regions of real solutions show patterns that are very similar to each other, and this feature was observed to be independent of the sequence and of the generation number. Also, the order of the generation plays an important role in the behaviour of the localization of the modes. A systematic study of the physical parameters was made, and we found that the size of the bulk bands is quite sensitive to the ratio $R$, although here we have obtained solutions even for $R > 1.0$ (or with structures which have a non-magnetic spacer with a thickness greater than that of the magnetic material) [21,28]. There exist other quasiperiodic sequences that can be studied as an extension of our work, following the procedures described here, such as the Cantor [26,31–33], the Rudin–Shapiro [26] and the random superlattices [26].

On the experimental side, the use of Brillouin scattering spectroscopy has proved to be an important tool for probing experimentally the theoretical predictions for these excitations [34]. Besides, a knowledge of the spectrum of the spin waves in a superlattice allows one to describe its linear response to an external source, such as an electromagnetic wave. The analysis can be done through the use of Green function techniques. Possible applications include spin valves and other multilayered devices.

## Acknowledgments

We would like to thank CNPq and CAPES (Brazilian agencies) and NSERC of Canada for partial financial support.

## Appendix A. Explicit form of the transfer matrix **T**

The transfer matrix **T** in equation (14) depends on the sequence and the generation considered. For the Fibonacci sequence, the matrix **T** for the $n$th generation is given iteratively by

$$\mathbf{T}_{S_{n+2}} = \mathbf{T}_{S_n}\mathbf{T}_{S_{n+1}} \tag{A.1}$$

where, for $n \geqslant 1$,

$$\begin{aligned} \mathbf{T}_{S_2} &= \mathbf{N}_\alpha^{-1}\mathbf{M}_k\mathbf{N}_k^{-1}\mathbf{M}_\alpha \\ \mathbf{T}_{S_1} &= \mathbf{M}_\alpha\mathbf{N}_\alpha^{-1}. \end{aligned} \tag{A.2}$$

For the Thue–Morse sequence, we have a slightly more complicated rule for the $n$th-generation **T** matrix:

$$\mathbf{T}_{S_n} = \mathbf{N}_\alpha^{-1}\mathbf{T}_{\mathrm{B}_n}\mathbf{T}_{\mathrm{A}_n}\mathbf{N}_\alpha \tag{A.3}$$

for $n \geqslant 1$, with

$$\mathbf{T}_{\mathrm{A}_{n+1}} = \mathbf{T}_{\mathrm{B}_n}\mathbf{T}_{\mathrm{A}_n} \tag{A.4}$$

$$\mathbf{T}_{\mathrm{B}_{n+1}} = \mathbf{T}_{\mathrm{A}_n}\mathbf{T}_{\mathrm{B}_n} \tag{A.5}$$

and

$$\mathbf{T}_{j_1} = \mathbf{M}_\xi\mathbf{N}_\xi^{-1}. \tag{A.6}$$

In the equation above, we consider ($j = \mathrm{A}, \xi = \alpha$) or ($j = \mathrm{B}, \xi = k$).

Finally, for the period-doubling sequence, we have ($n \geqslant 1$)

$$\mathbf{T}_{S_{n+2}} = \mathbf{T}_{S_n}\mathbf{T}_{S_n}\mathbf{T}_{S_{n+1}} \tag{A.7}$$

where

$$\mathbf{T}_{S_2} = \mathbf{T}_{S_0}\mathbf{T}_{S_0}\mathbf{T}_{S_1} \tag{A.8}$$

$$\mathbf{T}_{S_0} = \mathbf{N}_\alpha^{-1}\mathbf{M}_\alpha \tag{A.9}$$

$$\mathbf{T}_{S_1} = \mathbf{N}_\alpha^{-1}\mathbf{M}_k\mathbf{N}_k^{-1}\mathbf{M}_\alpha. \tag{A.10}$$

In all the equations above, the $2 \times 2$ matrices $\mathbf{N}_\xi$, $\mathbf{M}_\xi$ ($\xi = \alpha, k$) have the general form

$$\mathbf{M}_\xi = \begin{bmatrix} f_\xi & \bar{f}_\xi \\ \xi f_\xi & -\xi \bar{f}_\xi \end{bmatrix} \tag{A.11}$$

$$\mathbf{N}_\xi = \begin{bmatrix} 1 & 1 \\ \xi & -\xi \end{bmatrix} \tag{A.12}$$

where

$$f_\alpha = \mathrm{e}^{\alpha d_\mathrm{A}} \qquad \bar{f}_\alpha = 1/f_\alpha \tag{A.13}$$

$$f_k = \mathrm{e}^{k d_\mathrm{B}} \qquad \bar{f}_k = 1/f_k. \tag{A.14}$$

## References


[1] Shechtman D, Blench I, Gratias D and Cahn J W 1984 *Phys. Rev. Lett.* **53** 1951
[2] Kohmoto M and Banavar J R 1986 *Phys. Rev.* B **34** 563
[3] Sokoloff J B 1985 *Phys. Rep.* **126** 189
[4] Liu Y and Chao K A 1986 *Phys. Rev.* B **34** 5247
[5] Roy C L, Khan A and Basu C 1995 *J. Phys.: Condens. Matter* **7** 1843
[6] Roy C L and Khan A 1995 *Phys. Rev.* B **49** 14 949
Roy C L and Khan A 1995 *Phys. Lett.* A **196** 346
[7] Avishai Y and Berend D 1992 *Phys. Rev.* B **45** 2717
[8] Luck J M and Petritis D 1986 *J. Stat. Phys.* **42** 289
Riklund R and Severin M 1988 *J. Phys. C: Solid State Phys.* **21** L965
[9] Merlin R, Bajema K, Clarke R, Juang F-Y and Bhattacharya P K 1985 *Phys. Rev. Lett.* **55** 1768
[10] Todd J, Merlin R, Clarke R, Mohanty K M and Axe J D 1986 *Phys. Rev. Lett.* **57** 1157
[11] Thue A 1906 *K. Norske Vidensk. Selsk. Skr. Mat. Nat. Kl. Christiania* **7** 1
Thue A 1912 *K. Norske Vidensk. Selsk. Skr. Mat. Nat. Kl. Christiania* **13** 1
[12] Morse M 1921 *Trans. Am. Math. Soc.* **22** 84
[13] Axel F and Terauchi H 1991 *Phys. Rev. Lett.* **66** 2223
[14] Ghosh A and Karmakar S N 1998 *Phys. Rev.* B **57** 2834
[15] Süto A 1989 *J. Stat. Phys.* **56** 525
[16] Belisard J, Iochum B, Scoppola E and Testard D 1989 *Commun. Math. Phys.* **125** 527
Belisard J, Bovier A and Ghez J-M 1991 *Commun. Math. Phys.* **135** 379
[17] Kohmoto M, Sutherland B and Tang C 1987 *Phys. Rev.* B **35** 1020
[18] Ostlund S and Pandit R 1998 *Phys. Rev.* B **29** 1394
[19] Albuquerque E L 1993 *Phys. Lett.* A **181** 409
[20] Chakrabarti A, Karmakar S N and Moitra R K 1995 *Phys. Rev. Lett.* **74** 1403
[21] Cheng Z, Savit R and Merlin R 1988 *Phys. Rev.* B **37** 4375
[22] Sy H K and Chen Feng 1994 *Phys. Rev.* B **50** 3411
[23] Grünberg P 1989 *Light Scattering in Solids V* ed G Güntherodt and M Cardona (Heidelberg: Springer) p 303
[24] Feng J W, Jin G J, Hu A, Kang S S, Jiang S S and Feng D 1995 *Phys. Rev.* B **52** 15 312
[25] Bezerra C G and Albuquerque E L 1997 *Physica* A **245** 379
Bezerra C G and Albuquerque E L 1998 *Physica* A **255** 285
[26] Bezerra C G, Albuquerque E L and Nogueira E Jr 1999 *Physica* A **267** 124
[27] Mills D L 1984 *Surface Excitations* ed V M Agranovich and R Loudon (Amsterdam: North-Holland) p 379

[28] Camley R E and Cottam M G 1987 *Phys. Rev.* B **35** 189
[29] Anselmo D H A L, Cottam M G and Albuquerque E L 1999 *J. Appl. Phys.* **85** 5774
[30] Delyon F and Petritis D 1986 *Comment. Math. Phys.* **103** 441
[31] Vasconcelos M S and Albuquerque E L 1998 *Phys. Rev.* B **57** 2826
[32] de Oliveira P M C, Albuquerque E L and Mariz A M 1996 *Physica* A **227** 206
[33] Vasconcelos M S and Albuquerque E L 1996 *Physica* B **222** 113
[34] Borovik-Romanov A S and Kreines N M 1982 *Phys. Rep.* **81** 351